

Ultralow Thermal Conductivity in Full Heusler Semiconductors

Jiangang He,¹ Maximilian Amsler,¹ Yi Xia,² S. Shahab Naghavi,¹ Vinay I. Hegde,¹ Shiqiang Hao,¹ Stefan Goedecker,³ Vidvuds Ozoliņš,² and Chris Wolverton^{1,*}

¹*Department of Materials Science and Engineering, Northwestern University, Evanston, Illinois 60208, USA*

²*Department of Materials Science and Engineering, University of California, Los Angeles, California 90095, USA*

³*Department of Physics, Universität Basel, Klingelbergstrasse 82, 4056 Basel, Switzerland*

(Received 13 April 2016; published 21 July 2016)

Semiconducting half and, to a lesser extent, full Heusler compounds are promising thermoelectric materials due to their compelling electronic properties with large power factors. However, intrinsically high thermal conductivity resulting in a limited thermoelectric efficiency has so far impeded their widespread use in practical applications. Here, we report the computational discovery of a class of hitherto unknown stable semiconducting full Heusler compounds with ten valence electrons (X_2YZ , $X = \text{Ca, Sr, and Ba}$; $Y = \text{Au and Hg}$; $Z = \text{Sn, Pb, As, Sb, and Bi}$) through high-throughput *ab initio* screening. These new compounds exhibit ultralow lattice thermal conductivity κ_L close to the theoretical minimum due to strong anharmonic rattling of the heavy noble metals, while preserving high power factors, thus resulting in excellent phonon-glass electron-crystal materials.

DOI: 10.1103/PhysRevLett.117.046602

Limited fossil resources and environmental challenges have sparked an intense search for alternate methods for clean, sustainable, and efficient power generation in the last decade, with an increasing focus on thermoelectric (TE) materials for the direct conversion of electricity from (waste) heat [1]. The conversion efficiency is measured by the dimensionless figure of merit $ZT = S^2\sigma T / (\kappa_e + \kappa_L)$, where T is the absolute temperature, S is the thermopower, σ is the electrical conductivity, and κ_e and κ_L are the electronic and lattice thermal conductivities, respectively [2]. Optimizing ZT thus involves the tuning of conflicting material properties by maximizing the power factor (PF) σS^2 and minimizing thermal conductivity (κ_e and κ_L) simultaneously. The former is commonly achieved by band tuning and heavy doping, while the latter involves structural engineering through disorder (such as alloying Bi_2Te_3 [3]), complexity (such as Zn_4Sb_3 [4–6]), nanostructuring (such as PbTe [7]) or substructuring (skutterudites and clathrates [8–11]), anharmonicity ($\text{Cu}_{12}\text{Sb}_4\text{S}_{13}$ [12]), and ferroelectriclike lattice instability (SnSe [13,14]).

Semiconducting half Heusler (HH) compounds with XYZ composition and 18 valence electrons per formula unit (f.u.) have been recently actively studied as promising TE materials due to their excellent electronic and mechanical properties and thermal stability. ZT values as high as 1 have been reported for the n -type semiconductors XNiSn and XCoSb , $X = \{\text{Ti, Hf, Zr}\}$, and values exceeding 1 for p -type FeYSb , $Y = \{\text{V, Nb}\}$ at temperatures of about 1000 K (see Ref. [15], and references therein). The source of their compelling thermoelectric efficiency lies in the extremely high PF due to both the intrinsically narrow band gaps, which gives rise to a large σ , and the sharp increase in the density of states around the Fermi level, enhancing S

according to Mott's theory [16]. However, intrinsically high lattice thermal conductivity prevents a further improvement of ZT in HH materials. Although alloying and nanostructuring are actively used to increase phonon scattering, it has so far not been possible to reduce the thermal conductivity to values below $\kappa_L = 6.7 \text{ W m}^{-1} \text{ K}^{-1}$ at room temperature [17]. In a recent high-throughput *ab initio* study on 450 HH semiconductors merely four compounds were predicted to have κ_L of less than $5 \text{ W m}^{-1} \text{ K}^{-1}$ [18].

In contrast to HH compounds, only a few full Heusler (FH) materials with X_2YZ composition are semiconducting and have thus attracted limited attention as TE materials [19,20]. Although very high PFs at room temperature have been reported in FH compounds based on Fe_2VAl with values as high as $4\text{--}6 \text{ mW/m}^{-1} \text{ K}^{-2}$ [21–23], the effective ZT values are merely around 0.13–0.2 at 300 K [21,24,25] due to the high thermal conductivity (intrinsic $\kappa_L = 28 \text{ W/m}^{-1} \text{ K}^{-1}$ [21]). Recently, Bilc *et al.* predicted several FH compounds through bielemental substitution in Fe_2YZ , thereby demonstrating the possibility of boosting the PF by a factor of 5 through band engineering [26]. However, similar to HH compounds, the high thermal conductivity has so far prevented the use of known FH materials in efficient TE applications.

In conventional FH compounds, late transition metals commonly form the X_2 simple cubic sublattice and early transition metals and $\{\text{III, IV, V}\}$ main group elements are in the Y - Z rocksalt sublattice. It is well known that compounds with 24 valence electrons per f.u. can be semiconductors with fully occupied bonding states and empty antibonding states [27]. The electronic structure of such materials can be readily explained by orbital hybridization and crystal field splitting [20]. However, another

FH system that can be semiconducting and contains eight valence electrons per f.u. has been widely overlooked. These compounds do not contain transition metals and have only four fully occupied valence bands, e.g., Li_2NaSb and K_2CsSb [28].

To identify potential candidate materials with improved TE properties, we performed a high-throughput *ab initio* search for thermodynamically stable FH compounds with finite band gaps through elemental substitution within the QPMY [29] framework in a chemical search space with 53 distinct elements (see [30]). We discovered a class of stable semiconducting FH compounds with intrinsically high PFs and extremely low lattice thermal conductivity due to atomic rattling, which we call *R* Heusler compounds. These compounds, which to our knowledge have not yet been reported in the literature, contain ten valence electrons per f.u. with alkaline earth elements {Ba, Sr, Ca} in the *X* sublattice, whereas *Y* are noble metals {Au, Hg} and *Z* are main group elements {Sn, Pb, As, Sb, Bi}.

Density functional theory (DFT) calculations were performed within the projector augmented wave formalism [31] as implemented in the VASP [32,33] code together with the Perdew-Burke-Ernzerhof (PBE) approximation [34] to the exchange correlation potential [30]. Initially, the thermodynamic stability of all FH compounds was evaluated based on the convex hull taking into account all competing phases included in the open quantum materials database (OQMD) [35,36]. All *R* compounds have negative formation energies (-0.6 – -0.9 eV/atom) and were found to lie on the convex hull (see Table S1 [30]). However, even if a compound lies on the hull, there is still a possibility that a different crystal structure at given composition is lower in energy. We thus performed structural searches using the minima hopping method (MHM) as implemented in the MINHOCAO package [37,38]. MHM simulations were launched starting from the FH structure with up to 4 f.u. per cell in order to explore neighboring low-lying minima on the potential energy surface, visiting dozens of distinct minima per compound. Additionally, 18 intermetallic prototype structures were screened. Both searches did not yield any structures with energies lower than the Heusler phase for Ba containing compounds, indicating that they are thermodynamically stable. However, a distorted structure with $P21/m$ symmetry was found through the MHM which is favored for a few Sr and Ca compounds (see Table S2 in [30]), rendering them metastable. Since the energy differences between the $P21/m$ and Heusler structures are small, we expect that all *R* Heusler compounds are experimentally accessible, such that we will hereon focus solely on the Heusler phases. Furthermore, phonon calculations were carried out with the frozen phonon method as implemented in the PHONOPY package [39] to confirm that all Heusler phases are dynamically stable with no imaginary phonons (see Fig. S2 in [30]).

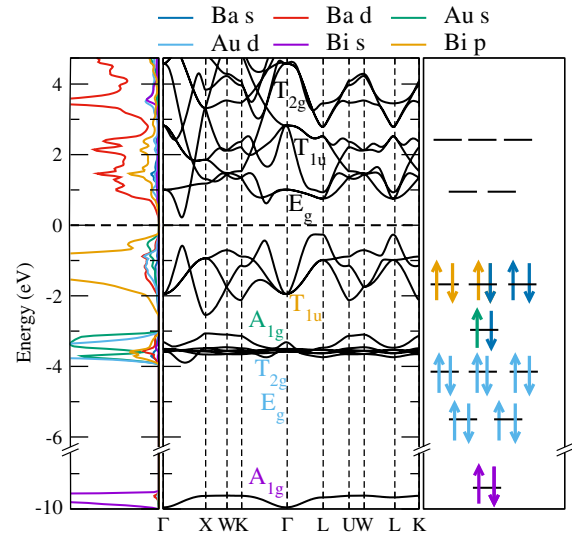


FIG. 1. Band structure and density of states (DOS) of cubic full Heusler ($Fm\bar{3}m$) Ba_2AuBi computed at the PBE level using the WIEN2K code [43] to extract the irreducible symmetry representation of each band at the Γ point.

Since semilocal DFT functionals are well known to underestimate band gaps, the screened HSE06 hybrid functional [40–42] was employed, leading to gaps between 0.01 (Ca_2AuBi) and 1.0 eV (Ba_2AuSb) (see Table S1), in the range of other good thermoelectrics. In Fig. 1 the band structure of Ba_2AuBi is shown as a representative case to illustrate how the *R* Heusler compounds lead to finite band gap materials. Near the Fermi level, the valence band is formed mainly by the Bi $6p$ orbitals and the conduction band is composed of the Ba $5d$ and Bi $6p^*$ states. The two most electropositive atoms Ba donate their four $5s$ electrons to the electronegative Au and Bi atoms. The fully occupied $5d$ and $6s$ states of the Au atom are extremely localized and far below the Fermi level, such that Au only weakly interacts with its neighboring atoms. This weak bonding gives rise to its unique vibrational behavior as will be discussed later. The Bi $6s$ lone pairs are buried deep below the Fermi level and are stereochemically inactive. Although the *R* compounds have in total ten valence electrons per f.u., these inactive Bi $6s$ lone pairs lead effectively to an eight-electron system, resulting in completely filled bonding and empty antibonding states in accordance with the electron counting rule to obtain a semiconductor.

The electronic transport properties of the *R* compounds were investigated to assess their quality as thermoelectric materials. Both the valence band maximum (VBM) and conduction band minimum (CBM) are at low symmetry points of the Brillouin zone. The VBM and CBM are located at the L and Δ point (between Γ and X) in the Brillouin zone, leading to high band degeneracy of 4 and 6, respectively. Furthermore, multiple bands have energies close to the VBM and CBM. Both properties lead to a sharp increase in the density of states around the Fermi level,

which is favorable for large Seebeck coefficients. Bilc *et al.* [26] recently showed that bands which are flat along one direction and highly dispersive along others lead to high PFs in FH materials. In fact, such bands are present in the new R compounds as well, where the valence band along L - Γ is flat, whereas it is highly dispersive along all other directions. To assess the thermoelectric conversion quality we solved the electronic Boltzmann transport equation within the constant relaxation time approximation using the BOLTZTRAP code [44]. The PBE band structures were resolved on a $41 \times 41 \times 41$ k -point mesh, and a constant shift of the bands was applied to open the gaps to the values obtained with the more accurate HSE06 functional [30]. Figure 2 compares the PFs of $X_2\text{AuBi}$ ($X = \text{Ba}$ and Sr) and the well-studied thermoelectric compound Fe_2VAl . In accordance with the work of Bilc *et al.* a constant relaxation time of $\tau = 3.4 \times 10^{-14}$ s was used. For n -doped Fe_2VAl , the maximum value of σS^2 lies at around $2.5 \text{ mW m}^{-1} \text{ K}^{-2}$, which is in good agreement with experimental and theoretical values [26]. A value of $6 \text{ mW m}^{-1} \text{ K}^{-2}$ is obtained for Ba_2AuBi at a similar carrier concentration. However, for p -type doping an even larger PF of $10 \text{ mW m}^{-1} \text{ K}^{-1}$ in Ba_2AuBi can be observed due to the “flat-and-dispersive” band at the L point.

Since all R Heusler compounds are semiconductors, the dominating term in the thermal conductivity stems from the lattice vibrations. The accurate estimation of the lattice thermal conductivity requires the calculation of phonon scattering intensities. Only the anharmonic part of the lattice dynamics contributes to phonon-phonon interactions. The recently developed compressive sensing lattice dynamics [45] technique was employed to obtain the third order force constants (FC). These FC were used to iteratively solve the linearized phonon Boltzmann equation with the SHENGBTE package [46]. Cutoff radii of 12 and 6 Å were used to truncate the 2- and 3-body interactions, respectively, resulting in values of κ_L converged to within $\pm 5\%$ (see Figs. S8 and S9 [30]). Although spin-orbit coupling (SOC) is known to influence the dynamical properties of materials containing heavy elements [47],

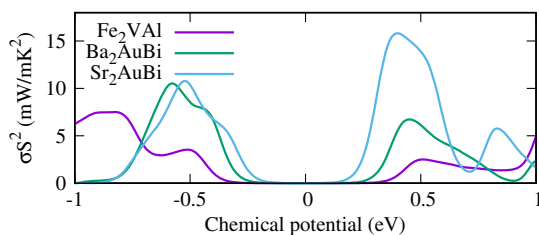


FIG. 2. PFs of the three FH compounds Ba_2AuBi , Sr_2AuBi , and Fe_2VAl at 300 K as a function of the electron chemical potential. Both n and p doping leads to significantly higher PFs of Ba_2AuBi and Sr_2AuBi compared to Fe_2VAl . For p doping, Ba_2AuBi and Sr_2AuBi have improved PFs due to the “flat-and-dispersive” valence bands.

our calculations show that the effect of SOC on the lattice thermal conductivity of the R Heusler compounds is negligible (see Fig. S11 [30]).

In Fig. 3 the intrinsic lattice thermal conductivities for all R compounds are shown as a function of temperature. All R Heusler compounds exhibit extremely low κ_L (0.5 – $1.5 \text{ W m}^{-1} \text{ K}^{-1}$ at 300 K), roughly one order of magnitude lower than previous experimental [17,21] and theoretical [18] values in other FH and HH materials. The lowest κ_L in Ba_2AuBi and Ba_2HgPb are even lower than $0.5 \text{ W m}^{-1} \text{ K}^{-1}$ at 300 K, which is comparable to the values along the out-of-plane direction of the van der Waals layers in SnSe ($\kappa_L = 0.47 \text{ W m}^{-1} \text{ K}^{-1}$), the material with the highest ZT known to date [13]. To verify the validity of the Boltzmann transport equation we computed the phonon mean free paths (MFP) at 300 K (see Fig. S4 [30]), indicating that the MFPs are overall longer than the smallest interatomic distances. However, we can expect that κ_L will eventually converge to the amorphous limit of $0.27 \text{ W m}^{-1} \text{ K}^{-1}$ (Cahill-Pohl model [48]) at higher temperatures. The discovery of such low values of κ_L is all the more exciting since only complex crystal structures with large unit cells, e.g., skutterudites and clathrates, were believed to give rise to strong resonant scattering [49]. Furthermore, we did not take into account additional phonon scattering mechanisms such as defects, dislocations, interfaces, and grain boundaries, which are known to additionally reduce the thermal conductivity. In fact, since FH and HH can be readily alloyed and nanostructured, we can expect a further reduction of κ_L in structurally engineered samples of Ba_2AuBi and Ba_2HgPb .

In order to understand the source of the extremely low lattice thermal conductivity we investigated the atomic

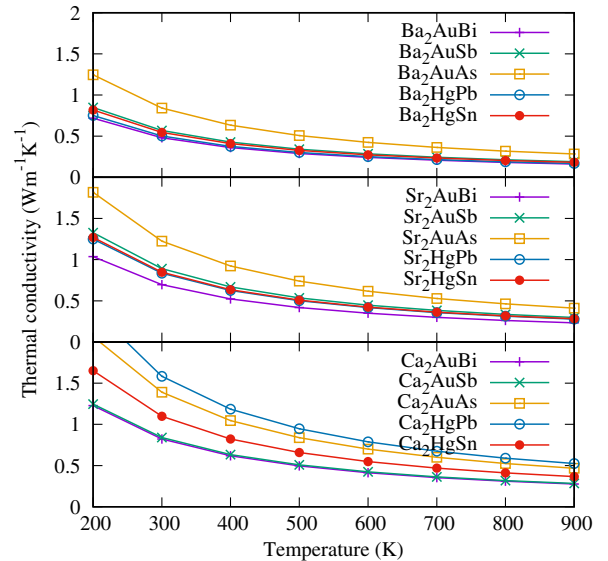


FIG. 3. Lattice thermal conductivity of the various Heusler compounds as a function of temperature. Each panel contains the compositions Ba_2YZ , Sr_2YZ , and Ca_2YZ , respectively.

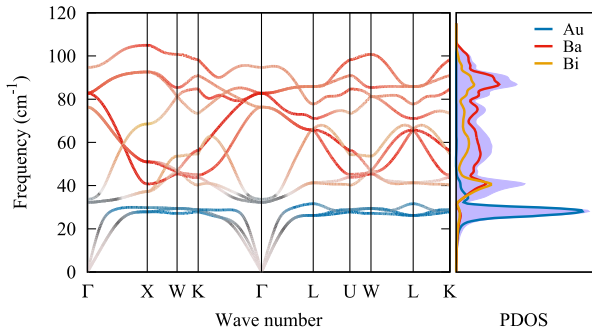


FIG. 4. The phonon band structures are shown in the left panel, taking into account LO/TO splitting. All bands are colored according to the amplitudes of the atomic eigendisplacements, where gray bands indicate an equal contribution of all atoms. The phonon density of states (PDOS) is plotted in the right panel, with the shaded area indicating the total DOS.

contribution to the phonons and their density of states (DOS). Since all R compounds have similar features in their phonon band structures (see Fig. S2 [30]), we will restrict our discussion to the material with the lowest lattice thermal conductivity, Ba_2AuBi . The band structure shown in Fig. 4 is colored according to the fractional amplitudes of the mode eigenvectors of each atom, indicating that flat, low-energy acoustic modes (around 25 cm^{-1}) are dominated by Au vibrations (blue), whereas optical branches are exclusively governed by Ba and Bi atoms (red and orange) (see also Fig. S10 [30]). In fact, the avoided crossing of the acoustic and optical branches is a clear indication of atomic rattling. Such strong rattling behavior with similar vibrational properties has so far only been observed in clathrates and skutterudites, which are well known for their low thermal conductivities where guest atoms rattle in the host cage structures and scatter the heat-carrying phonons [50–56]. Analogously to clathrates, the low energy phonon branches can be interpreted as Au atoms rattling in a pseudocage structure composed of the alkali and main group atoms (X and Z) (see Fig. S3 [30]). As discussed above, the strongly localized $6s$ state lead to weak interactions with the $6p$ states of the Z -site atoms, such that Au behaves like the inert alkaline (earth) metals in clathrate cages.

The mode dependent phonon lifetime τ shows a dip at $\omega \approx 35 \text{ cm}^{-1}$, another indication of strong rattling according to the resonant scattering model [49] (see Fig. S3 [30]). The strong influence of the rattling modes on κ_L can be seen in Fig. 5, where the scattering rates Γ^\pm for the three-phonon interaction of both the absorption processes (Γ^+ for $\lambda + \lambda' \rightarrow \lambda''$) and emission processes (Γ^- for $\lambda \rightarrow \lambda' + \lambda''$) are shown [57]. Here, we used $\lambda \equiv (\alpha, \mathbf{q})$ to describe phonons with branch index α and wave vector \mathbf{q} . As expected from the resonant scattering model, there is a strong contribution to Γ^+ due to rattling (left segment), but the rattlers also interact with the optical modes in the emission processes (right segment, Γ^-), which additionally

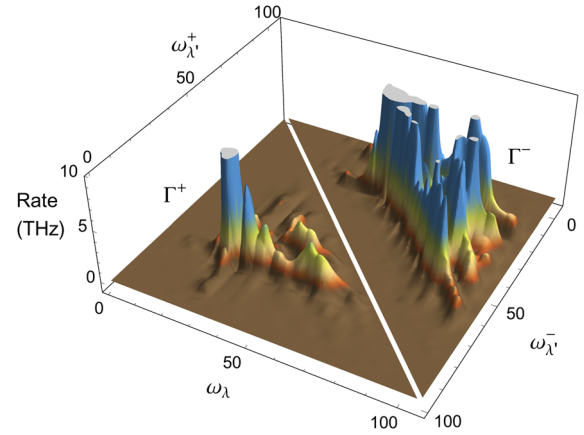


FIG. 5. Scattering rates Γ^+ and Γ^- for Ba_2AuBi at 300 K. The left segment shows the absorption rates, whereas the right panel indicates the rates for emission processes. The corresponding phonon frequencies ω are given in units of cm^{-1} .

impedes the transport of heat carried by optical phonons. Furthermore, there are two general chemical trends that can be observed in Fig. 3. First, the overall value of κ_L decreases strongly with each period of the alkali earth metal elements X_2 . This behavior can be simply attributed to the size of the X element, which, depending on its radius, creates larger or smaller voids for the Y atoms, giving it more or less space to rattle. Second, and to a lesser extent, κ_L decreases with the overall phonon frequencies at a given element X (see Fig. S2 [30]), which is a direct consequence of the mass of the Z element.

In summary, we predict a new class of thermodynamically stable FH semiconductors with excellent thermoelectric properties from first principles calculations. The electronic transport properties are comparable to the well-studied thermoelectric FH compound Fe_2VAl with high PFs due to flat-and-dispersive valence bands. Unlike known FH and HH compounds, our novel FH compounds have one order of magnitude lower lattice thermal conductivities, comparable to the value of SnSe . The heavy noble metals Au and Hg are only weakly bonded such that they can freely rattle in the pseudocages composed of the nearest and next-nearest neighbors. Consequently, the strong scattering of the heat carrying acoustic phonons leads to a suppression of the thermal conductivity to values comparable to glass, which could be further reduced through structural engineering. In strong contrast to the common perception that only complex or host-guest structures with large unit cells can lead to such low thermal conductivity [49], R Heusler compounds demonstrate that ultralow thermal conductivity can be realized in very simple crystal structures. These properties not only establish the novel R Heusler compounds as very promising thermoelectric materials, but will, moreover, lead to fundamental advances in the design of novel materials for thermoelectric applications. Experimental synthesis of the R Heusler compounds is called for to verify our predictions.

J. H. and C. W. acknowledge support via ONR STTR N00014-13-P-1056. M. A. gratefully acknowledges support from the Novartis Universität Basel Excellence Scholarship for Life Sciences and the Swiss National Science Foundation. Y. X., S. S. N., and V. O. acknowledge support by the U.S. Department of Energy, Office of Science, Basic Energy Sciences, under Grant No. DE-FG02-07ER46433. V. I. H. acknowledges support from NSF Grant No. DMR-1309957. S. H. acknowledges support by the U.S. Department of Energy, Office of Science, Office of Basic Energy Sciences, under Award No. DE-SC0014520. Computational resources from the Swiss National Supercomputing Center (CSCS) in Lugano (Projects No. s499 and No. s621) and the National Energy Research Scientific Computing Center, which is supported by the Office of Science of the U.S. Department of Energy under Contract No. DE-AC02-05CH11231, are acknowledged.

J. H. and M. A. contributed equally to this work.

*c-wolverton@northwestern.edu

- [1] G. J. Snyder and E. S. Toberer, *Nat. Mater.* **7**, 105 (2008).
- [2] D. Rowe, *Thermoelectrics Handbook: Macro to Nano* (CRC Press, Boca Raton, 2005).
- [3] D. A. Wright, *Nature (London)* **181**, 834 (1958).
- [4] G. J. Snyder, M. Christensen, E. Nishikori, T. Caillat, and B. B. Iversen, *Nat. Mater.* **3**, 458 (2004).
- [5] L. Bjerg, G. K. H. Madsen, and B. B. Iversen, *Chem. Mater.* **23**, 3907 (2011).
- [6] L. Bjerg, B. B. Iversen, and G. K. H. Madsen, *Phys. Rev. B* **89**, 024304 (2014).
- [7] H. J. Wu, L.-D. Zhao, F. S. Zheng, D. Wu, Y. L. Pei, X. Tong, M. G. Kanatzidis, and J. Q. He, *Nat. Commun.* **5**, 4515 (2014).
- [8] T. Tadano, Y. Gohda, and S. Tsuneyuki, *Phys. Rev. Lett.* **114**, 095501 (2015).
- [9] C. Uher, in *Semiconductors and Semimetals*, Recent Trends in Thermoelectric Materials Research I Vol. 69, edited by T. M. Tritt (Elsevier, San Diego, 2001), pp. 139–253.
- [10] G. S. Nolas, G. A. Slack, and S. B. Schujman, in *Semiconductors and Semimetals* (Ref. [9]), pp. 255–300.
- [11] G. S. Nolas, J. Poon, and M. Kanatzidis, *MRS Bull.* **31**, 199 (2006).
- [12] X. Lu, D. T. Morelli, Y. Xia, F. Zhou, V. Ozoliņš, H. Chi, X. Zhou, and C. Uher, *Adv. Energy Mater.* **3**, 342 (2013).
- [13] L.-D. Zhao, S.-H. Lo, Y. Zhang, H. Sun, G. Tan, C. Uher, C. Wolverton, V. P. Dravid, and M. G. Kanatzidis, *Nature (London)* **508**, 373 (2014).
- [14] C. W. Li, J. Hong, A. F. May, D. Bansal, S. Chi, T. Hong, G. Ehlers, and O. Delaire, *Nat. Phys.* **11**, 1063 (2015).
- [15] T. Zhu, C. Fu, H. Xie, Y. Liu, and X. Zhao, *Adv. Energy Mater.* **5**, 1500588 (2015).
- [16] A. M. Rao, X. Ji, and T. M. Tritt, *MRS Bull.* **31**, 218 (2006).
- [17] S. Chen and Z. Ren, *Mater. Today* **16**, 387 (2013).
- [18] J. Carrete, W. Li, N. Mingo, S. Wang, and S. Curtarolo, *Phys. Rev. X* **4**, 011019 (2014).
- [19] F. Heusler, *Verh. Dtsch. Phys. Ges.* **5**, 219 (1903).
- [20] I. Galanakis, P. H. Dederichs, and N. Papanikolaou, *Phys. Rev. B* **66**, 174429 (2002).
- [21] Y. Nishino, S. Deguchi, and U. Mizutani, *Phys. Rev. B* **74**, 115115 (2006).
- [22] M. Vasundhara, V. Srinivas, and V. V. Rao, *Phys. Rev. B* **77**, 224415 (2008).
- [23] E. J. Skoug, C. Zhou, Y. Pei, and D. T. Morelli, *J. Electron. Mater.* **38**, 1221 (2009).
- [24] Y. Terazawa, M. Mikami, T. Itoh, and T. Takeuchi, *J. Electron. Mater.* **41**, 1348 (2012).
- [25] M. Mikami, Y. Kinemuchi, K. Ozaki, Y. Terazawa, and T. Takeuchi, *J. Appl. Phys.* **111**, 093710 (2012).
- [26] D. I. Bilc, G. Hautier, D. Waroquiers, G.-M. Rignanese, and P. Ghosez, *Phys. Rev. Lett.* **114**, 136601 (2015).
- [27] T. Graf, C. Felser, and S. S. Parkin, *Prog. Solid State Chem.* **39**, 1 (2011).
- [28] C. Felser and A. Hirohata, *Heusler Alloys: Properties, Growth, Applications* (Springer, New York, 2015).
- [29] QMPY (suite of computational materials science tools), <https://pypi.python.org/pypi/qmpy>.
- [30] See Supplemental Material at <http://link.aps.org/supplemental/10.1103/PhysRevLett.117.046602> for details on the computational methods employed in this work. Furthermore, detailed descriptions of the thermodynamic stabilities, prototype crystal structures, phonon dispersion, phonon lifetimes and mean free paths, electronic band structure, effect of spin-orbit coupling, convergence tests, and power factors are presented, along with Tables S1–S4 and Figs. S1–S12.
- [31] P. E. Blöchl, *Phys. Rev. B* **50**, 17953 (1994).
- [32] G. Kresse and J. Furthmüller, *Comput. Mater. Sci.* **6**, 15 (1996).
- [33] G. Kresse and D. Joubert, *Phys. Rev. B* **59**, 1758 (1999).
- [34] J. P. Perdew, K. Burke, and M. Ernzerhof, *Phys. Rev. Lett.* **77**, 3865 (1996).
- [35] J. Saal, S. Kirklin, M. Aykol, B. Meredig, and C. Wolverton, *JOM* **65**, 1501 (2013).
- [36] S. Kirklin, J. E. Saal, B. Meredig, A. Thompson, J. W. Doak, M. Aykol, S. Rhl, and C. Wolverton, *npj Comput. Mater.* **1**, 15010 (2015).
- [37] S. Goedecker, *J. Chem. Phys.* **120**, 9911 (2004).
- [38] M. Amsler and S. Goedecker, *J. Chem. Phys.* **133**, 224104 (2010).
- [39] A. Togo, F. Oba, and I. Tanaka, *Phys. Rev. B* **78**, 134106 (2008).
- [40] J. Heyd, G. E. Scuseria, and M. Ernzerhof, *J. Chem. Phys.* **118**, 8207 (2003).
- [41] J. Paier, M. Marsman, K. Hummer, G. Kresse, I. C. Gerber, and J. G. Ángyán, *J. Chem. Phys.* **125**, 249901 (2006).
- [42] J. Heyd, G. E. Scuseria, and M. Ernzerhof, *J. Chem. Phys.* **124**, 219906 (2006).
- [43] P. Blaha, K. Schwarz, P. Sorantin, and S. B. Trickey, *Comput. Phys. Commun.* **59**, 399 (1990).
- [44] G. K. Madsen and D. J. Singh, *Comput. Phys. Commun.* **175**, 67 (2006).
- [45] F. Zhou, W. Nielson, Y. Xia, and V. Ozoliņš, *Phys. Rev. Lett.* **113**, 185501 (2014).
- [46] W. Li, J. Carrete, N. A. Katcho, and N. Mingo, *Comput. Phys. Commun.* **185**, 1747 (2014).
- [47] M. J. Verstraete, M. Torrent, F. Jollet, G. Zrah, and X. Gonze, *Phys. Rev. B* **78**, 045119.

- [48] D. G. Cahill and R. O. Pohl, *Annu. Rev. Phys. Chem.* **39**, 93 (1988).
- [49] E. S. Toberer, A. Zevalkink, and G. J. Snyder, *J. Mater. Chem.* **21**, 15843 (2011).
- [50] G. S. Nolas, J. L. Cohn, G. A. Slack, and S. B. Schujman, *Appl. Phys. Lett.* **73**, 178 (1998).
- [51] J. L. Cohn, G. S. Nolas, V. Fessatidis, T. H. Metcalf, and G. A. Slack, *Phys. Rev. Lett.* **82**, 779 (1999).
- [52] N. P. Blake, L. Møllnitz, G. Kresse, and H. Metiu, *J. Chem. Phys.* **111**, 3133 (1999).
- [53] J. Dong, O. F. Sankey, G. K. Ramachandran, and P. F. McMillan, *J. Appl. Phys.* **87**, 7726 (2000).
- [54] J. Dong, O. F. Sankey, and C. W. Myles, *Phys. Rev. Lett.* **86**, 2361 (2001).
- [55] J. S. Tse, Z. Li, and K. Uehara, *Europhys. Lett.* **56**, 261 (2001).
- [56] Y. He and G. Galli, *Nano Lett.* **14**, 2920 (2014).
- [57] N. Mingo, D. A. Stewart, D. A. Broido, L. Lindsay, and W. Li, in *Length-Scale Dependent Phonon Interactions*, Topics in Applied Physics No. 128, edited by S. L. Shind and G. P. Srivastava (Springer, New York, 2013), pp. 137–173.